NEUROSCIENCE

Presynaptic Black Box Opened by Pioneers at Biophysics Department in University College London

Tomoyuki Takahashi

Cellular and Molecular Synaptic Function Unit, Okinawa Institute of Science and Technology (OIST) Graduate University, Okinawa 904-0495, Japan

Abstract—The mechanism of chemical synaptic transmission was elucidated at the frog neuromuscular junction (NMJ) and at the squid giant synapse by Katz, Miledi and other researchers. Later progress in molecular biology revealed numerous types of proteins in mammalian central synapses. To establish molecular–functional correlation in synaptic transmission, it now seems essential to re-address the fundamental mechanisms at mammalian central synapses. Using patch-clamp whole-cell recording at the calyx of Held in slices of rodent brainstem, we have identified quantal EPSCs and reproduced the quantal analysis established at the NMJ. Intra-terminal whole-cell loading of the neurotransmitter, glutamate, revealed that vesicular transmitter content is an important determinant of quantal size and its variation. Regarding the Ca^{2+}-dependence of transmitter release, the average coupling distance between Ca^{2+} entry sites and exocytic vesicles was estimated as tens of nanometers and was found to undergo developmental tightening at the calyx of Held. Numerical simulations suggested that this distance can determine the synaptic delay, synchronicity of vesicular transmitter release, and release probability. The super-linear input (presynaptic)–output (postsynaptic) relationship of neurotransmission is an important physiological feature discovered at squid giant synapses. However, at the calyx of Held, unlike at the squid synapse, the input–output relationship had a wide safety margin, protecting transmitter release from a diminishment of presynaptic action potentials. As in the NMJ, Ca^{2+} remaining in the cytosol after action potential facilitates subsequent release. As a downstream mechanism of this residual Ca^{2+}, a Ca^{2+}-induced Ca^{2+} channel activation via high-affinity Ca^{2+} binding proteins was discovered at mammalian central synapses. *This article is part of a Special Issue entitled: Honoring Ricardo Miledi - outstanding neuroscientist of XX-XXI centuries.* © 2019 The Author(s). Published by Elsevier Ltd on behalf of IBRO. This is an open access article under the CC BY-NC-ND license (http://creativecommons.org/licenses/by-nc-nd/4.0/).

Key words: quantum hypothesis, synaptic vesicle, Ca^{2+} channel, neuromuscular junction, calyx of Held, input–output relationship.

INTRODUCTION

After the controversies regarding electrical or chemical nature of synaptic transmission were settled, the mechanisms of chemical transmission were extensively studied by Bernard Katz and colleagues at the Biophysics Department, University College London (UCL), during the period from 1950 to 1980, using frog NMJ and squid stellate ganglion synapses. Major discoveries from the laboratory include the quantal nature of synaptic transmission, the triggering role of Ca^{2+} entry for transmitter release, the facilitatory role of residual Ca^{2+}, the non-linear input–output relationship between presynaptic and postsynaptic compartments, and the postsynaptic receptor-channel mechanisms. Many attempts were made thereafter to extend the concept of chemical transmission, established at these synapses, to mammalian central synapses. To this end, it was recognized essential to establish a simple mammalian synapse preparation, where signals from a single presynaptic input and postsynaptic current responses could be monitored simultaneously, as in the squid giant synapse. The calyx of Held in acute slices of rodent brainstem has provided such preparation. In this review, I summarize how the classic concepts from the frog NMJ and squid synapses, have been re-addressed at the calyx of Held in the author's laboratory.

Quantal nature of central synaptic transmission

The "accidental" discovery of spontaneous miniature end-plate potentials (mEPPs) at the frog NMJ (Fatt and Katz, 1951; Katz, 1993) inspired Katz and colleagues at UCL to raise the quantum hypothesis of transmitter release (Del Castillo and Katz, 1954a). Extension of this hypothesis to central synapses was not straightforward, however, because of the complex synaptic organizations in the brain. Small potential blips like mEPPs occur spontaneously in CNS

neurons, but they were regarded as 'synaptic noise' (Eccles, 1961) arising from spontaneous firing of surrounding cells. In 1963, Katz and Miledi (1963) recorded spontaneous synaptic potentials from motoneurons of isolated frog spinal cord, after blocking synaptic transmission with high [MgCl₂] or [KCl] in bath solutions (Fig. 1A). Intracellular recording with K citrate-filled electrode revealed depolarizing and hyperpolarizing blips, which were judged to be miniature excitatory and inhibitory postsynaptic potentials (mEPSPs, mIPSPs), respectively (Fig. 1Aa). Replacement of Cl^- with SO_4^{2-} permitted to isolate mEPSPs with skewed amplitude profiles (Fig. 1Ab). This was the first demonstration of quantal synaptic responses in central synapses. Extension of these findings to mammalian central synapses was subsequently made by Blankenship and Kuno (1968), who blocked APs using tetrodotoxin (TTX) applied to spinal motoneurons of anesthetized cat and recorded miniature synaptic potentials. Later, miniature events were recorded from motoneurons of isolated rat spinal cord in the presence of TTX (Fig. 1B, Takahashi, 1984). These events were abolished by strychnine, suggesting that they were mIPSPs produced by the inhibitory transmitter, glycine. The absence of mEPSPs could be attributed to remote dendritic location of excitatory inputs, distant from the recording site. These mIPSPs behaved like mEPPs, with their frequency increased by raising extracellular Ca^{2+} concentration, K^+ concentration, or osmotic pressure (Kojima and Takahashi, 1985).

Unlike the mEPPs at the NMJ, mIPSPs in rat spinal motoneurons originate from multiple inputs. Since the quantal size may vary from one input to another, they cannot be used for quantal analysis of synaptic responses from a given input. This inability to identify input-specific quantal events at central synapses made quantal analyses rely on multiple peak distributions of the evoked synaptic potentials or currents (Edwards et al., 1990; Larkman et al., 1992; Jonas et al., 1993), but none of them reached a clear conclusion (Kuno, 1995). An attempt to extract quantal events that constitute evoked responses was made using extracellular [Ca^{2+}] / [Mg^{2+}] titration for the amplitude of IPSCs recorded from rat spinal motoneurons in slices (Takahashi, 1992). When the [Ca^{2+}] / [Mg^{2+}] ratio was reduced by steps, the amplitude of IPSC decreased to a minimal steady level that unveiled the quantal size (Fig. 2A, 2B). Likewise, in immature rat cerebellar slices, evoked quantal EPSCs, resistant to [Ca^{2+}] / [Mg^{2+}] changes, were occasionally observed, suggesting that they derived from single release-sites (Silver et al., 1996, Fig. 2C). These "minimal evoked responses" are considered quantal events, distinct from multi-quantal responses evoked by minimal stimulation (Allen and Stevens, 1994). Eventually, variance–mean analysis was established by Clements and Silver (2000) as a standard quantal analysis method. This method is based upon binomial amplitude distribution of synaptic responses and allows to estimate quantal parameters from a parabolic curve fit to data points of evoked PSCs at different release probabilities obtained for example by changing [Ca^{2+}] / [Mg^{2+}] ratio (Fig. 2D). In this method the mean quantal size (Q_W) is estimated from the initial slope of parabola; the number of release sites (N) from the PSC amplitude at the maximal release probability (P_r), and P_r is calculated from the PSC amplitude divided by N, according to the quantum hypothesis (PSC amplitude = NP_rQ_W, Del Castillo and Katz, 1954a).

Patch-clamp techniques (Hamill et al., 1981) applied to mammalian central neurons (Edwards et al., 1989) visualized in thin slices (Takahashi, 1978), enabled stable pair recordings simultaneously from pre- and postsynaptic structures at the rodent calyx of Held (Borst et al., 1995; Takahashi et al., 1996) (Fig. 3A). The single glutamatergic input permits to analyze the spontaneous EPSCs as equivalent to mEPSCs. In fact, TTX has no effect on the amplitude distribution or mean frequency of the spontaneous EPSCs (Ishikawa et al., 2002). In simultaneous pre- and postsynaptic recording, stepwise presynaptic depolarizations increase the frequency of mEPSCs without affecting their amplitude profile (Fig. 3B) (Sahara and Takahashi, 2001), as in mEPPs at the frog NMJ (Del Castillo and Katz, 1954b). Although postsynaptic receptors were proposed to be saturated by transmitter
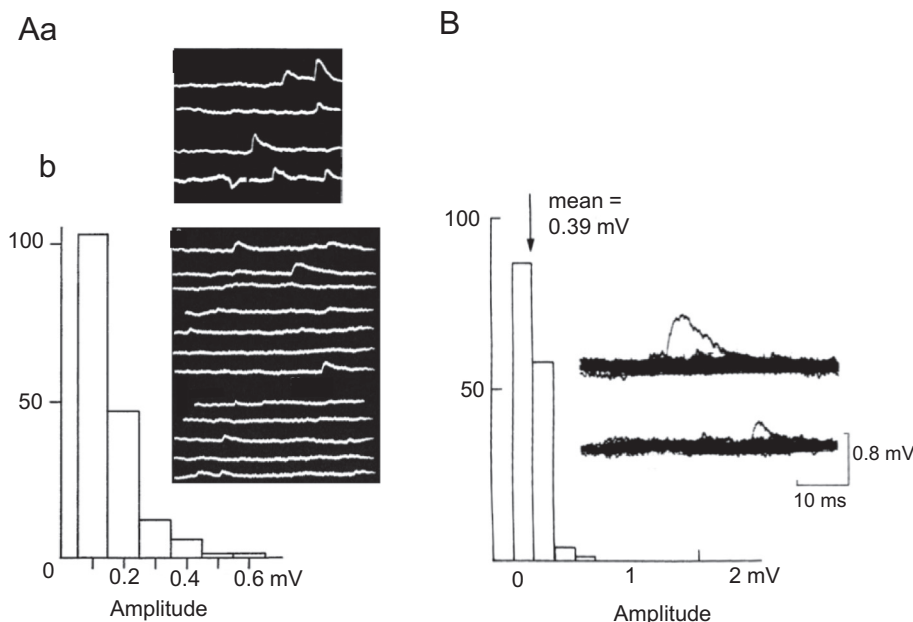

Fig. 1. Spontaneous miniature synaptic responses at CNS synapses. **(Aa)** Spontaneous mEPSPs and mIPSPs recorded from a frog spinal motoneuron using K citrate-filled microelectrode. **(Ab)** mEPSPs recorded in chloride-deficient "sulfate" Ringer. Ordinate in amplitude histogram indicates number of events. Adopted with permission from Katz and Miledi, 1963. **(B)** Spontaneous mIPSPs recorded from an immature rat spinal motoneuron using KCl filled microelectrode. Ten traces are superimposed. Adopted with permission from Takahashi, 1984.
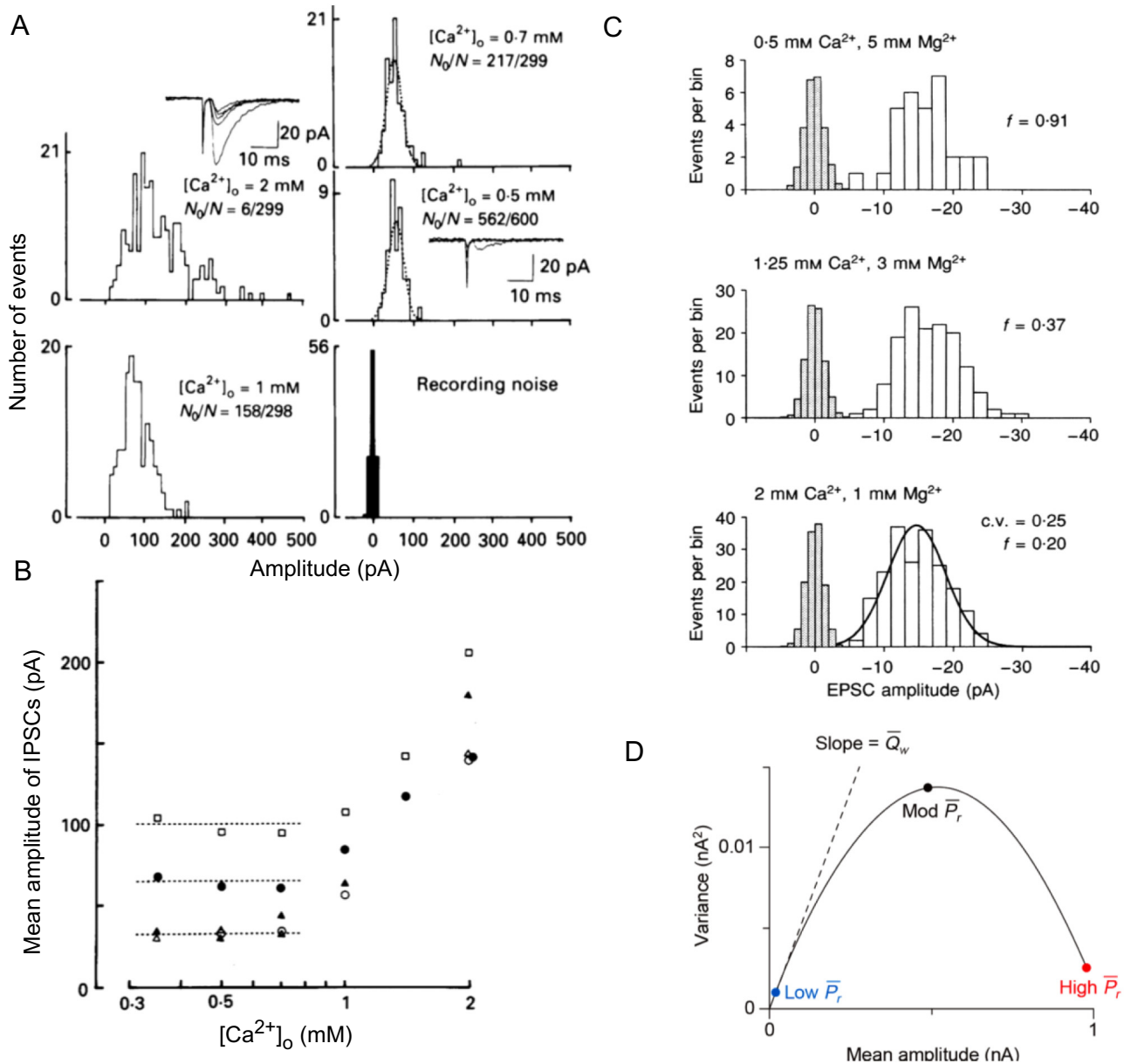
Fig. 2. Quantal synaptic currents revealed as the minimal evoked currents. **(A)** Minimal evoked IPSCs recorded using patch-clamp whole-cell techniques from a motoneuron in spinal cord slices of an immature rat. **(B)** Mean amplitude of IPSCs at different $[Ca^{2+}]$, revealing the minimal evoked IPSC amplitudes in 5 motoneurons. Adopted with permission from Takahashi, 1992. **(C)** Amplitude histograms of EPSCs recorded at a putative single-site cerebellar mossy fiber-granule cell synapse at different $[Ca^{2+}]$ / $[Mg^{2+}]$ ratios. Filled columns indicate background noise levels. Adopted with permission from Silver et al., 1996. **(D)** Variance–mean analysis. P_r, release probability (in response to single AP) calculated from mean EPSC amplitude divided by maximum EPSC amplitude; Q_w, mean quantal amplitude estimated from the initial slope (variance / mean). The equation for parabola; $y = Ax - Bx^2$. Adopted with permission from Clements and Silver, 2000.

(Jack et al., 1981; Larkman et al., 1992; Jonas et al., 1993), transmitter glutamate does not normally saturate postsynaptic AMPA receptors at the calyx of Held (Ishikawa et al., 2002). Glutamate infused at high concentrations into presynaptic terminals increased the amplitude of mEPSC, ie quantal size, without changing the kinetics of mEPSCs (Fig. 3C). The mean amplitude of mEPSCs was larger when glutamate was loaded at higher concentrations (Fig. 3D). Non-saturation of postsynaptic AMPA receptors by quantal transmitter is also suggested for hippocampal synapses in culture

from experiments using a low-affinity AMPA receptor agonist (Liu et al., 1999).

A long-standing question has been which factor determines the variations in the quantal size (Katz, 1993). When many quanta are released synchronously, glutamate can saturate postsynaptic AMPA receptors. The coefficient of variation (cv = variance / mean) of such EPSC amplitudes is as small as 0.04 at the cerebellar mossy fiber-granule cell synapse (Silver et al., 1996). In contrast, the cv of quantal size was 0.4 at the calyx of Held (Sahara and Takahashi, 2001), or
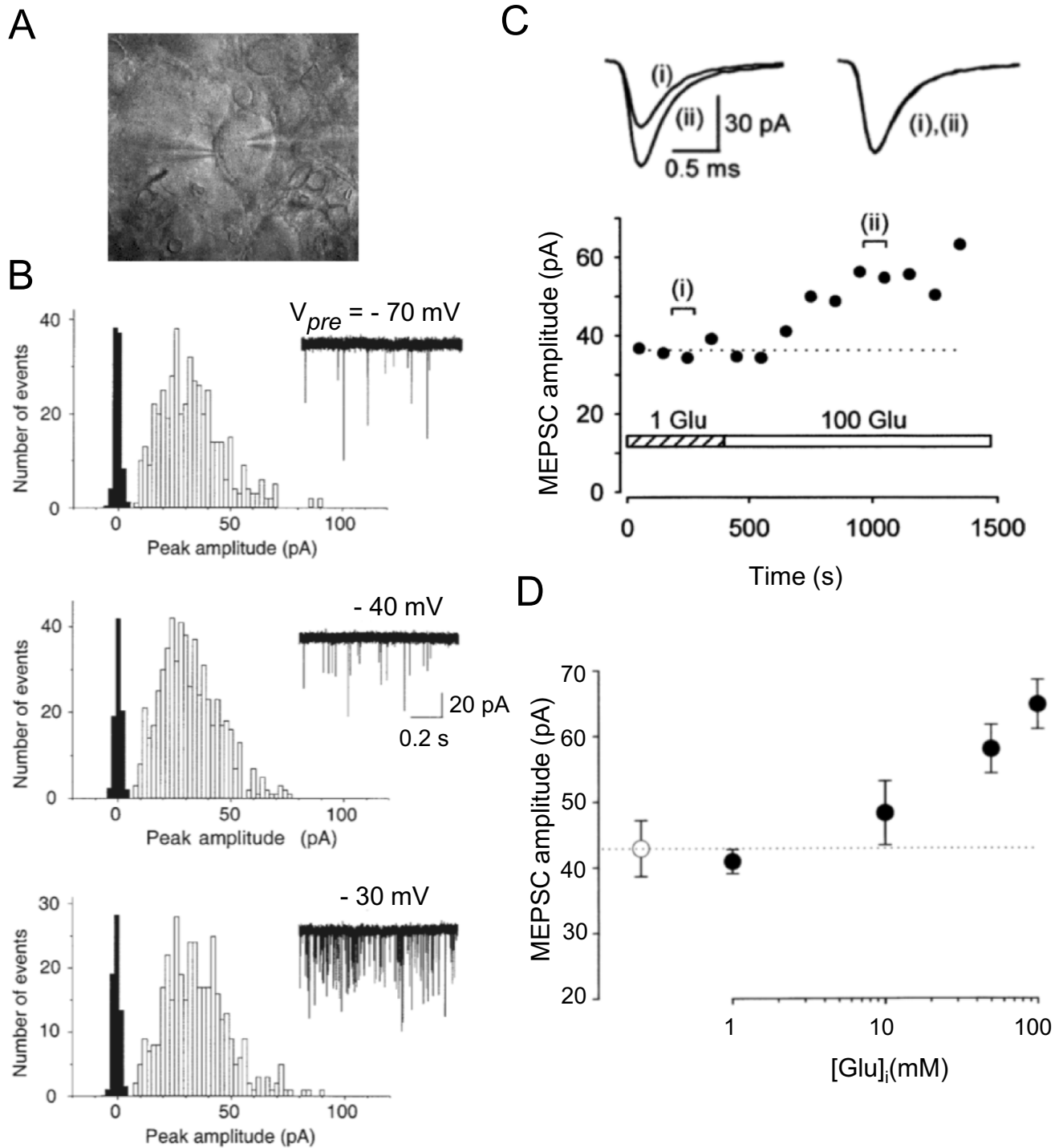
Fig. 3. Glutamatergic mEPSCs characterized using simultaneous pre- and postsynaptic whole-cell recording at the calyx of Held. **(A)** Paired whole-cell recording at the calyx of Held. Presynaptic currents are recorded from a calyceal terminal (left patch pipette), while postsynaptic currents are recorded from a principal neuron in the medial nucleus of trapezoid body (right pipette). **(B)** Unchanged mEPSC amplitude profiles at different presynaptic membrane potentials produced by current injections (−70 mV, −40 mV, and − 30 mV, from top to bottom). MEPSCs increased their frequencies in response to presynaptic depolarization. Adopted with permission from Sahara and Takahashi, 2001. **(C)** An increase in mEPSC amplitude in response to elevation of cytosolic [glutamate] from 1 mM to 100 mM using patch pipette perfusion. Sample traces are averaged mEPSCs in 1 mM (i) and 100 mM (ii) cytosolic [glutamate] (superimposed). The two traces completely overlap when their amplitude is normalized, indicating no change in kinetics (right traces). **(D)** Mean mEPSC amplitudes at different cytosolic [glutamate]. An open circle indicates mean amplitude of mEPSCs at the calyx of Held without presynaptic whole-cell perturbation. **(C)** and **(D)** adopted with permission from Ishikawa et al., 2002.

at the inhibitory synapse in motoneurons (Takahashi, 1992), and 0.2–0.3 at cerebellar mossy fiber single-site synapses (Silver et al. 1996). Since postsynaptic receptors are not saturated by a quantum of transmitter (Ishikawa et al., 2002), these quantal size variations likely arise primarily from variation of vesicular transmitter contents, and secondarily from inter-site variation of postsynaptic receptor densities (but see Liu et al., 1999). Presynaptic whole-cell dialysis experiments indicate that vesicular transmitter content is in dynamic equilibrium with that in cytosol (Ishikawa et al., 2002; Hori and Takahashi, 2012; Takami et al., 2017; Yamashita et al., 2018). This can explain a run-down of postsynaptic potential amplitude at a cholinergic synapse of *Aplysia* after intracellular injection of acetylcholine esterase (Tauc, 1982), which was regarded as evidence against the quantal/vesicular hypothesis.

At both glutamatergic (Herman et al., 2014) and GABAergic (Wang et al., 2013) synapses in culture, vesicular transmitter contents are reported to affect the number of quanta released by a presynaptic AP (quantal content).

However, in experiments where vesicular transmitter content was decreased or increased, by manipulating cytosolic transmitter concentrations, exocytic capacitance changes of presynaptic membrane remained the same, at both glutamatergic synapses (Fig. 4A, 4B) (Hori and Takahashi, 2012; Takami et al., 2017) and GABAergic synapses (Fig 4C) (Yamashita et al., 2018). Thus, empty or poorly filled vesicles can undergo exocytosis as efficiently as fully filled vesicles. Other conflicting evidence to the quantum hypothesis comes from sub-miniature EPPs observed at the frog NMJ, particularly after tetanic stimulation (Kriebel, 1978). These events might arise from incompletely filled synaptic vesicles, as refilling of synaptic vesicles with neurotransmitter is a slow process, with tens of seconds in time constants, at both excitatory (Hori and Takahashi, 2012) and inhibitory (Yamashita et al., 2018) synapses.

The quantal nature of chemical synaptic transmission has been established at the frog NMJ (Del Castillo and Katz, 1954a) based on the findings of evoked EPPs to Poisson's law in a low $[Ca^{2+}]$/high $[Mg^{2+}]$ solution (Fig. 5A). Del Castillo and Katz demonstrated that (i) the amplitude histogram of EPPs fits with integer multiples of mEPP amplitude histogram, assuming Poisson's law, and (ii) quantal sizes calculated from two independent methods agree ($\log_e$ (number of trials) / (number of failures) = (EPP amplitude) / (mEPP amplitude) (Del Castillo and Katz, 1954a). This classical quantal analysis was reproduced at a central inhibitory synapse in leech (Nicholls and Wallace, 1978), and more recently at the calyx of Held of rodents for glutamatergic EPSCs (Sahara and Takahashi, 2001) (Fig. 5B). Thus, the quantum hypothesis originally raised at the frog NMJ does hold at this mammalian central synapse.
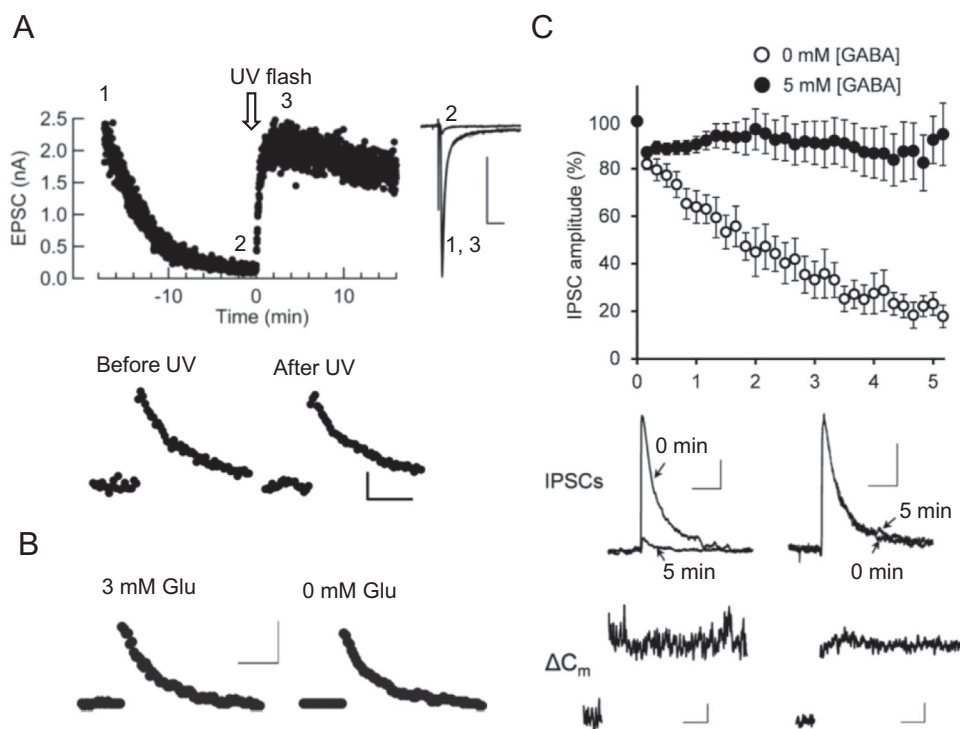

Fig. 4. The vesicular filling state has no effect on the number of vesicles released per AP. **(A)** Experiments at the calyx of Held. The evoked EPSC amplitude declined after whole-cell washout of cytosolic glutamate. Subsequent UV photo-release of glutamate from caged compound MNI-glutamate recovered the EPSC amplitude. Sample traces (right superimposed) represent EPSCs before and after glutamate uncaging. Lower panels, in separate experiments, exo-endocytic membrane capacitance changes were induced by presynaptic Ca^{2+} currents. No difference between before (left, glutamate-deficient) and after (right, glutamate-filled) uncaging. Calibrations, 1 nA, 5 ms for EPSCs and 50 fF, 10s for capacitance. Adopted with permission from Hori and Takahashi, 2012. **(B)** No difference in presynaptic membrane capacitance changes before and after cytosolic glutamate washout at the calyx of Held. Calibration, 0.2 pF, 10s. Adopted with permission from Takami et al., 2017. **(C)** Whole-cell GABA washout in cerebellar Purkinje cell terminals in culture reduced amplitudes of IPSCs evoked by Ca^{2+} currents and recorded from postsynaptic deep nuclear cells. Sample traces in the middle panels are IPSCs before and 5 min after GABA washout (superimposed left traces) or 5 mM GABA loading (right traces, superimposed). Exocytic capacitance changes (ΔC_m) 5 min after GABA washout (left) or 5 mM GABA loading show no significant difference. Calibrations, 50 pA, 100 ms for left panel IPSCs and 20 pA, 100 ms for right panel IPSCs, and 100 pA, 5 ms for capacitance traces. Adopted with permission from Yamashita et al., 2018. Quantitative data in cited references.
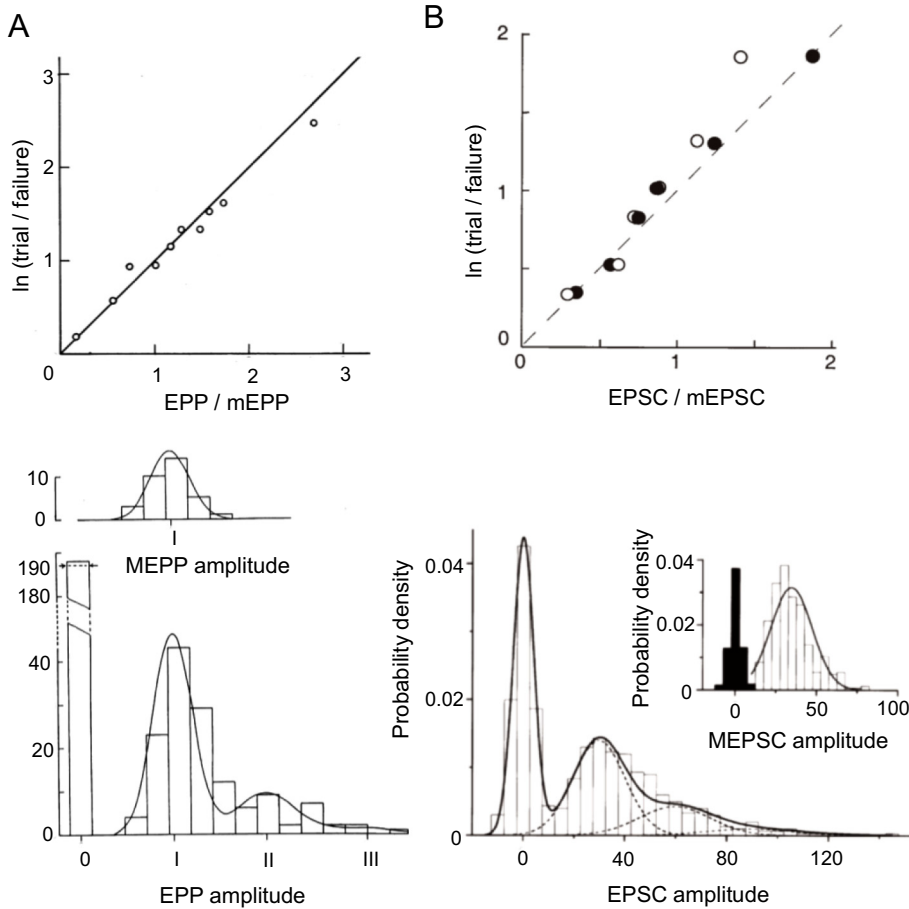
Calcium-release coupling clarified at giant synapses in squid and rodents

The importance of extracellular Ca^{2+} for synaptic transmission has been widely recognized since 1940s (Feng, 1988) and its effect on transmitter release was demonstrated at the NMJ (Del Castillo and Stark, 1952). However, for some time, it remained unclear whether Ca^{2+} acts at outside or inside of nerve terminals. Whereas

Fig. 5. Quantal nature of transmitter release at NMJ and CNS synapses. (A) *Top panel*, coincidence in quantal sizes calculated from ln (number of trials / number of failures) (ordinate) and EPP/mEPP amplitude ratio (abscissa). *Middle panel*, the mEPP amplitude histogram. *Bottom panel*, the EPP amplitude histogram fit by a curve predicted from Poisson's law. Modified Adopted with permission from Del Castillo and Katz, 1954a. (B) *Upper panel*, coincident quantal sizes calculated from ln (number of trials / number of failures) (ordinate) and EPSC/mEPSC amplitude ratio (abscissa) at the calyx of Held. *Lower panel,* the EPSC amplitude histogram fit by a curve predicted from Poisson's law. Inset, the mEPSC amplitude histogram. Adopted with permission from Sahara and Takahashi, 2001.

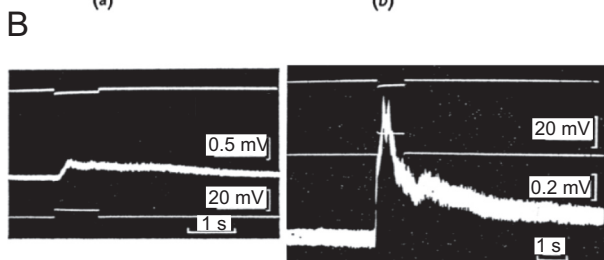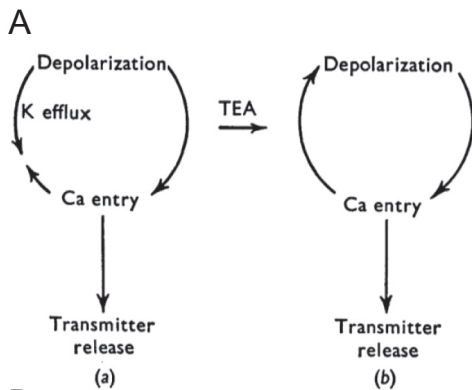iontophoretic Ca^{2+} injection to the squid giant presynaptic terminals failed to induce postsynaptic responses (Miledi and Slater, 1966), Katz and Miledi (1969) found that pharmacological block of K$^+$ channels with tetra-ethyl ammonium (TEA) induces a regenerative Ca^{2+} entry, similar to Na$^+$ entry during an AP (Hodgkin and Huxley, 1952). Based on these observations they suggested that Ca^{2+} enters through voltage-gated Ca^{2+} channels and exerts its action inside the nerve terminal to trigger transmitter release (Fig. 6A). Quantitative analyses on this issue were made later at this synapse (Llinas et al., 1976). Eventually, Miledi (1973) demonstrated that iontophoretic Ca^{2+} application from a microelectrode inserted into a squid giant presynaptic terminal produces asynchronous transmitter release (Fig. 6B). Later studies using Ca^{2+} indicators at squid synapses demonstrated that Ca^{2+} entry does occur near the release sites of squid giant synapses (Augustine et al., 1985; Llinas et al., 1992).

The spatial distribution of Ca^{2+} channels and its influence on transmitter release were systematically examined at the calyx of Held of developing rats (Nakamura et al., 2015). Immunogold freeze-fracture replica labeling of Cav2.1 (P/Q-type Ca^{2+} channel) has revealed Ca^{2+} channel clusters of various sizes, comprising 2–27 channels, on the synaptic face of the terminal (Fig. 7A). When an AP was elicited with a whole-cell patch pipette at a calyceal terminal, a fast Ca^{2+} transient was recorded, with a short delay, at confocal optical spots along the distal edge of the terminal, where transmitter is released (Fig. 7B). At spots opposite to the release face, Ca^{2+} transients were small and slow, suggesting that Ca^{2+}

Fig. 6. Neurotransmitter release is triggered by elevated [Ca^{2+}] in presynaptic terminals. (A) Diagram illustrating the 'calcium hypothesis', applied to the squid giant presynaptic terminal treated with TTX. Transmitter release is normally triggered by Ca^{2+} influx adjusted by K$^+$ efflux. When K$^+$ conductance is blocked with TEA, Ca^{2+} entry becomes regenerative via positive-feedback between presynaptic depolarization and Ca^{2+} entry. Adopted with permission from Katz and Miledi, 1969. (B) Two examples of postsynaptic responses induced by iontophoretic application of Ca^{2+} from a microelectrode inserted into a squid presynaptic terminal. Traces from top to bottom; iontophoretic Ca^{2+} pulse, postsynaptic potential, presynaptic potential. Adopted with permission from Miledi, 1973.
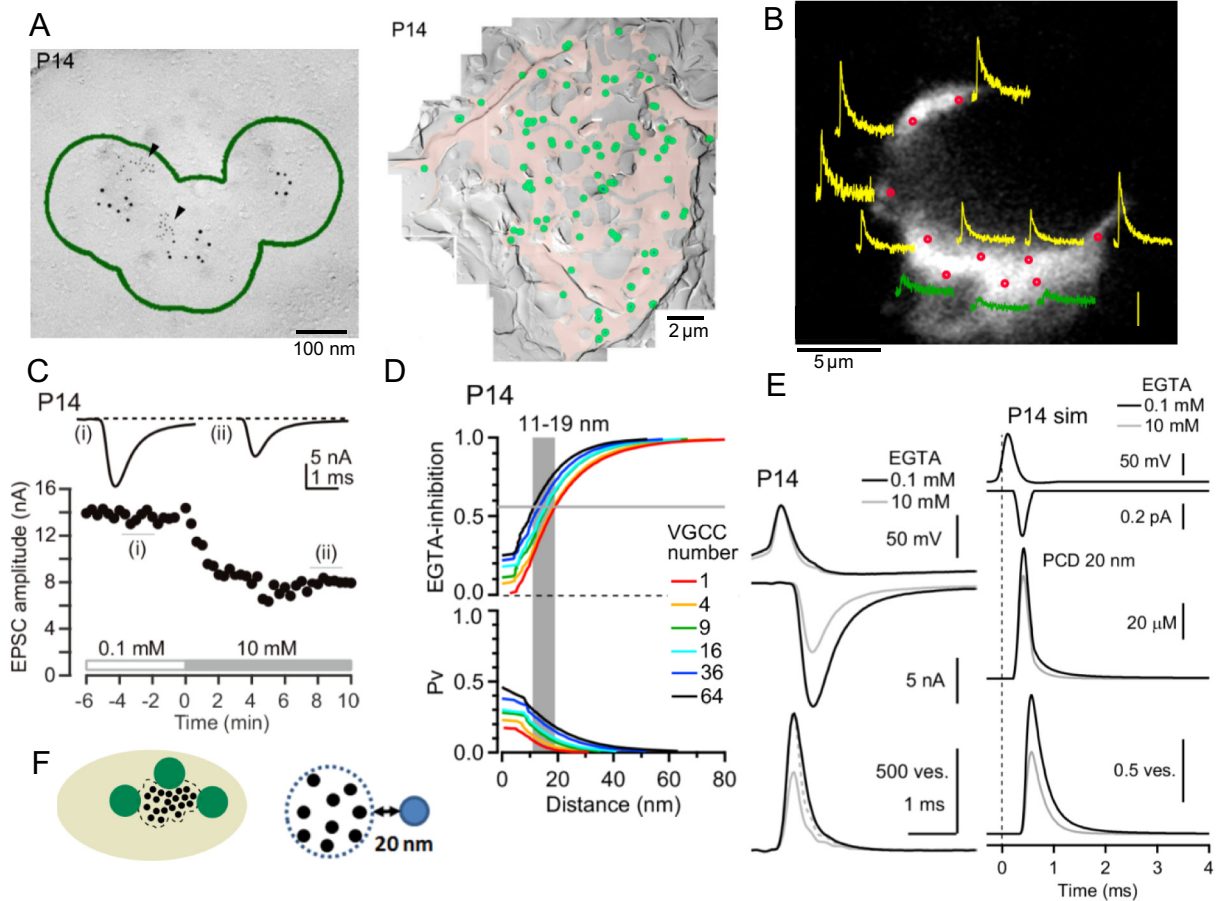
Fig. 7. Ca^{2+}-release coupling at the calyx of Held presynaptic terminal. **(A)** *Left panel*, a Cav2.1 (P/Q type Ca^{2+}-channel) cluster in the presynaptic terminal revealed by freeze-fracture replica immune-gold labeling (5 nm diameter) using a specific antibody. Double-labeled Rim 1 particles (2 nm diameter) co-exist in the Cav2.1 cluster defined by a green contour (for definition of cluster, see Nakamura et al., 2015, Supplemental Information). *Right panel*, Many Cav2.1 clusters (green) distributed on the P-face (release face, pink) of a calyceal terminal. **(B)** AP-induced Ca^{2+} transients detected at confocal spots (red) with Oregon green BAPTA-5 N loaded into the calyx terminal (calyx is visualized using Alexa 594). Yellow and green traces are Ca^{2+} transients recorded from spots on the synaptic face and non-synaptic regions, respectively. **(C)** Effect of intra-terminal EGTA perfusion on EPSC amplitude. [EGTA] in presynaptic patch pipette was switched from 0.1 mM to 10 mM using pipette perfusion. Upon infusion of 10-mM EGTA, EPSC amplitude gradually declined and reached a steady low level within several minutes. Sample traces of EPSCs before and after switching [EGTA] to 10 mM are shown on the top panel. **(D)** Numerical simulation based upon a model. Various numbers of Ca^{2+} channels in a cluster (1–64) are assumed and color-coded. Ordinates indicate the fraction of EPSC amplitude inhibited by 10 mM EGTA (upper panel) and vesicular release probability (P_v, lower panel). Abscissae indicate distance (in nm) from the nearest perimeter of a Ca^{2+} channel cluster to an exocytic vesicle (PCD). Gray shadow is set by the data from EGTA experiments (~50% reduction at P14). This gives PCD values of 11–19 nm and P_v of <0.3, depending on the number of Ca^{2+} channels in a cluster. The PCD value is relatively stable for a wide range of intra-cluster Ca^{2+} channel numbers. **(E)** AP, EPSCs and release rate (at 0.1 and 10 mM EGTA, superimposed) obtained by deconvolution of EPSCs with mEPSCs from P14 calyx (left traces). Right traces are simulated AP (mV), Ca^{2+} currents (nA), intra-terminal $[Ca^{2+}]$ changes (μM) and release rate (vesicle number, at 0.1 and 10 mM EGTA, superimposed), based on the perimeter release model assuming PCD as 20 nm (right traces). **(F)** Left, imaginary active zone topography of Ca^{2+} channels (black) in a cluster and exocytic synaptic vesicles docked at release sites (green). Right, a scheme of perimeter release model. Adopted with permission from Nakamura et al., 2015.

seen with intracellular dye was derived from remote entry sites. The Ca^{2+}-release coupling distance can be estimated from the effect of presynaptic loading of a Ca^{2+} chelator EGTA (K_{on} = 1.5 mM^{-1} ms^{-1}) on EPSC amplitude. Presynaptic EGTA (2 mM) attenuated EPSC amplitude by ~ 60% at calyces of Held of postnatal day (P) 14 rats (Fig. 7C). Numerical simulations based upon this and other data, including estimation of intracellular Ca^{2+} buffer strength and kinetics, suggested that the coupling distance between a release site and a perimeter of a Ca^{2+} channel cluster to be ~20 nm at P14 (Fig. 7D). The vesicular release probability

(P_v) estimated by the simulation from perimeter coupling distance (PCD) agreed well with the reported value estimated using variance–mean analysis (Koike-Tani et al., 2008). Furthermore, the vesicular release rate and synaptic delay estimated from the simulation coincided well with recorded data (Fig. 7E). Based on these findings, a Ca^{2+}-release coupling model was proposed, in which release sites are located tens of nanometers distant from the perimeter of a Ca^{2+} channel cluster (Fig. 7F). This coupling distance shortened from 30 nm to 20 nm during postnatal development from P7 to P14 (Nakamura et al., 2015).
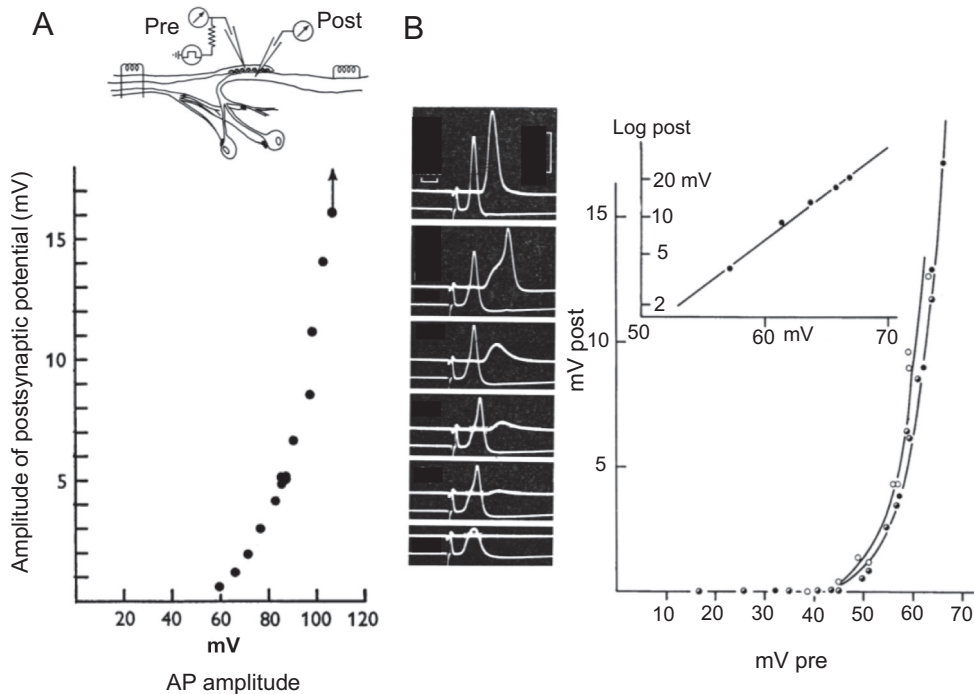
Fig. 8. Input–output relationship at the squid giant synapse. **(A)** EPSP amplitude (ordinate) is plotted against presynaptic AP amplitude (abscissa) altered by presynaptic polarization and depolarization. The upper drawing illustrates the experimental set-up at the squid synapse. Adopted with permission from Miledi and Slater, 1966. **(B)** Same as **(A)** but AP amplitude was diminished by TTX application. *Left panel,* simultaneous recording of presynaptic APs and EPSP during TTX application (from top to bottom). *Right graph,* input–output relationship. The inset graph is a semilogarithmic plot showing the slope of the relationship. Adopted with permission from Katz and Miledi, 1967.

The input–output relationship at giant synapses in squid and rodents

The input–output relationship at synapses is a fundamental issue, which determines informational flow through neuronal circuitry. At squid giant synapses, slight alteration of presynaptic AP amplitude by changing membrane potential (Hagiwara and Tasaki, 1958; Takeuchi and Takeuchi, 1962; Miledi and Slater, 1966), or with tetrodotoxin (TTX) at a low concentration (Katz and Miledi, 1967), causes large changes in postsynaptic response amplitude (Fig 8A, 8B). Specifically, changing presynaptic AP amplitude by 14–20 mV causes a 10-fold change of postsynaptic response amplitude (Miledi and Slater, 1966; Katz and Miledi, 1967) (Fig. 8A, 8B). Such a super-linear input–output relationship is thought to explain the presynaptic inhibition caused by depolarization of primary afferent terminals in the mammalian spinal cord (Eccles, 1964). These experiments are presently feasible at the mammalian synapse, calyx of Held, where the input–output relationship can be examined using simultaneous pre- and postsynaptic whole-cell recording (Hori and Takahashi, 2009). When TTX was applied at a low concentration, the amplitude of the presynaptic AP gradually declined, but the EPSC amplitude remained similar until the AP overshoot dropped below +10 mV (Fig. 9A). Below this level, a 10-mV reduction in presynaptic AP amplitude diminished EPSC amplitude by 72%, as it happens in the squid synapse

(86%, Katz and Miledi, 1967). When AP amplitude was increased by up to 30% by presynaptic hyperpolarization, EPSC amplitude did not change (Fig. 9B). Thus, the input–output relationship at the calyx of Held synapse is different from that at the squid giant synapse (Hagiwara and Tasaki, 1958; Miledi and Slater, 1966). This wide safety margin observed at the calyx of Held is produced by broadening of the reduced presynaptic APs (Hori and Takahashi, 2009).

In *Aplysia*, a presynaptic depolarization facilitates transmitter release (Klein and Kandel, 1978), whereas in mammalian spinal cord, presynaptic depolarization is thought to depress transmitter release (Eccles, 1961). Does presynaptic depolarization facilitate or inhibit transmitter release at the calyx of Held? This question was addressed by increasing the extracellular [KCl] (Fig. 9C). In these experiments, input fibers were stimulated to evoke EPSCs in a neuron unperturbed with presynaptic pipettes (synapse #1) and presynaptic APs were recorded from a neighboring presynaptic terminal (synapse #2). Elevation of extracellular [KCl] to 12.5 mM slowly depolarized presynaptic terminals, in association with a gradual decline in presynaptic AP amplitude (synapse #2). Concomitantly, the EPSC amplitude increased and then decreased (synapse #2). The initial EPSC facilitation is likely caused by presynaptic Ca^{2+} current facilitation (Cuttle et al., 1998, Fig. 10). This Ca^{2+} current facilitation occurs specifically for Cav2.1 (P/Q type Ca^{2+} channels (Ishikawa et al., 2005). Residual Ca^{2+} (Katz and Miledi, 1968) then binds to the high affinity Ca^{2+} binding protein, neuronal calcium sensor 1 (Tsujimoto et al., 2002) or calmodulin (DeMaria et al., 2001), thereby accelerating Ca^{2+} channel activation kinetics (Fig. 10A). This effect accounts for paired-pulse facilitation by ~ 50% at the calyx of Held (Fig. 10B) (Muller et al., 2008; Hori and Takahashi, 2009), and by nearly 100% at cerebellar inhibitory synapses between Purkinje neurons (Diaz-Rojas et al., 2015). At the calyx of Held, this function is augmented by a developmental switch of Ca^{2+} channels from Cav2.2 (N type) to Cav2.1 (P/Q type) (Iwasaki and Takahashi, 1998; Ishikawa et al., 2005). During presynaptic depolarization by KCl, synaptic facilitation is switched to depression when presynaptic AP overshoot was diminished below +10 mV (Fig. 9D). Thus, the wide
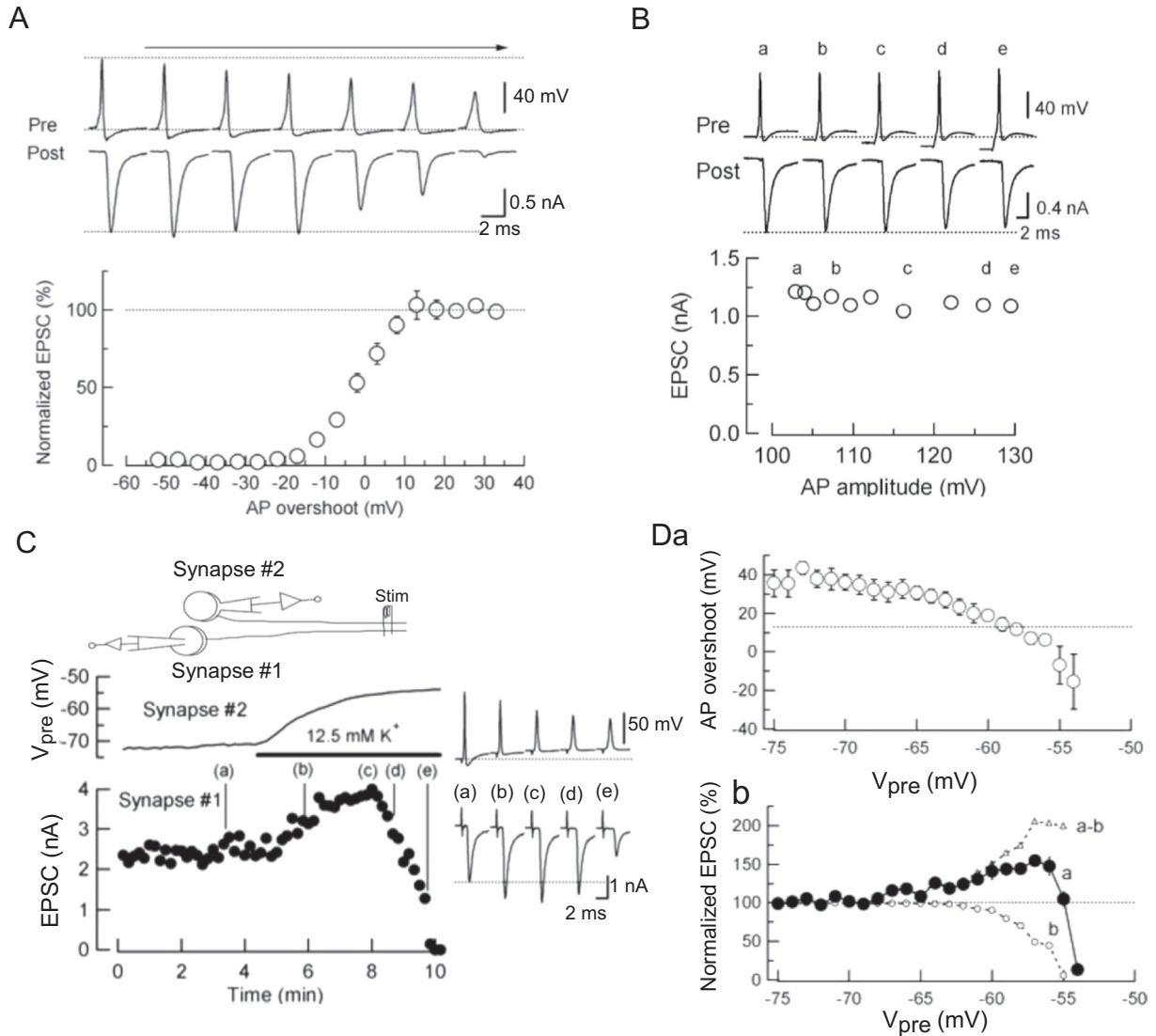
Fig. 9. Input–output relationship at the calyx of Held. **(A)** Amplitudes of EPSCs (ordinate) and presynaptic APs (abscissa). Upper records show presynaptic APs and EPSCs during TTX application (10 nM). **(B)** Amplitudes of EPSCs (ordinate) and presynaptic AP overshoot (abscissa). Presynaptic AP was enlarged to ~130% by hyperpolarization, but EPSC amplitude remained unchanged. Upper and lower records are presynaptic APs and EPSCs, respectively. Hyperpolarizing currents were injected into a presynaptic terminal. Note increased presynaptic resting potentials from the initial level (dashed line) and similar EPSC amplitudes (dashed line, a–e). **(C)** Effect of external [KCl] elevation on EPSC amplitude. *Top illustration*, EPSCs were recorded from a postsynaptic neuron (synapse #1) with no presynaptic pipette. APs were recorded from a nearby presynaptic terminal (synapse #2). Input fiber stimulations evoked EPSCs at synapse #1 and presynaptic APs at synapse #2 in an all-or-none fashion, but with different thresholds, indicating that two different fibers are stimulated (for details, see Hori and Takahashi, 2009). **(D)** Biphasic effects of presynaptic depolarization on EPSC amplitude. **(Da)** Presynaptic AP overshoot amplitude plotted against presynaptic membrane potential (synapse #2). As presynaptic terminals were depolarized by [KCl] elevation, presynaptic AP amplitude gradually declined. A dashed line indicates the minimal level of AP overshoot inducing full size EPSCs in the TTX experiments (A). **(Db)** Relative EPSC amplitude (synapse #1) plotted against presynaptic membrane potential (synapse #2). Open circles (curve b) indicate EPSC amplitudes estimated from AP size reductions **(Da)** and its effect on EPSC amplitudes expected from data in Fig. 9A. Open triangles (curve a–b) indicate EPSC amplitudes obtained by subtracting data b from data a, representing components of EPSCs facilitated during presynaptic depolarization. Adopted with permission from Hori and Takahashi, 2009.
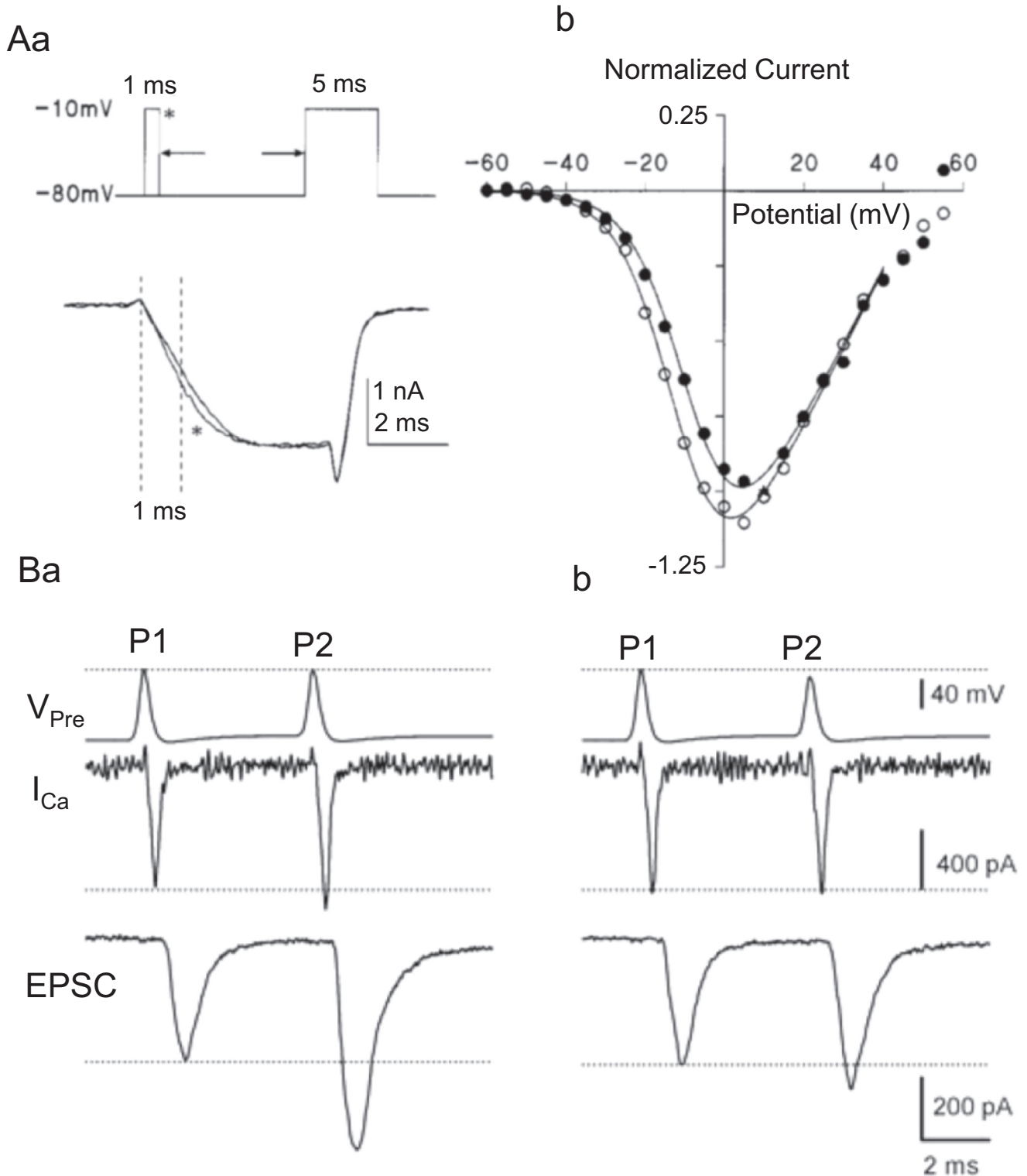
Fig. 10. Facilitation of presynaptic Ca^{2+} currents. **(Aa)** Acceleration of Ca^{2+} current rise time by a conditioning pulse (1 ms, applied 10 ms before 5-ms test pulse, voltage command protocol, indicated with *left top trace*). *Lower traces*, Ca^{2+} currents with or without conditioning pulse (superimposed) showing rise time acceleration by the depolarizing conditioning pulse. **(Ab)** Ca^{2+} current–voltage relationships measured 1 ms from the test pulse onset, with (open circles) or without (filled circles) a depolarizing conditioning pulse. Adopted with permission from Cuttle et al., 1998. **(Ba)** Paired-pulse facilitation of EPSCs evoked by a pair of AP waveform-induced Ca^{2+} currents (P1 and P2) with 5-ms inter-pulse intervals, in the presence of botulinum toxin E (20 nM) and 0.5 mM EGTA in presynaptic pipette to minimize synaptic depression. Traces from top to bottom indicate AP-waveform command pulses, presynaptic Ca^{2+} currents, and EPSCs, respectively. Ca^{2+} current facilitation induced by paired-pulse stimulation facilitated EPSCs. **(Bb)** Presynaptic AP waveform command pulse at P2 was manually adjusted by reduction just to cancel Ca^{2+} current facilitation. This significantly reduced paired-pulse facilitation of EPSCs, revealing a contribution of Ca^{2+} current facilitation to synaptic facilitation. Adopted with permission from Hori and Takahashi, 2009.

safety margin of input–output relationship contributes to facilitation of transmitter release during presynaptic depolarization at this mammalian synapse.

Studies of neurotransmitter release at frog NMJ and squid synapses established the fundamental mechanistic concepts for chemical synaptic transmission. Re-examination of the presynaptic mechanisms at the mammalian central synapse, calyx of Held, confirmed such fundamental mechanisms and revealed distinct mechanisms. Given the wealth of molecular resources, experimental tools and information available at mammalian synapses, a molecular functional clarification of mammalian presynaptic regulatory mechanisms is a promising field of neuroscience research.

ACKNOWLEDGMENTS

REFERENCES

Allen C, Stevens CF. (1994) An evaluation of causes for unreliability of synaptic transmission. Proc Natl Acad Sci U S A 91:10380-10383.

Augustine GJ, Charlton MP, Smith SJ. (1985) Calcium entry into voltage-clamped presynaptic terminals of squid. J Physiol 367:143-162.

Blankenship JE, Kuno M. (1968) Analysis of spontaneous subthreshold activity in spinal motoneurons of the cat. J Neurophysiol 31:195-209.

Borst JGG, Helmchen F, Sakmann B. (1995) Pre- and postsynaptic whole-cell recordings in the medial nucleus of the trapezoid body of the rat. J Physiol 489:825.

Clements JD, Silver RA. (2000) Unveiling synaptic plasticity: a new graphical and analytical approach. TINS 23:105-113.

Cuttle MF, Tsujimoto T, Forsythe ID, Takahashi T. (1998) Facilitation of the presynaptic calcium current at an auditory synapse in rat brainstem. J Physiol 512:723-729.

Del Castillo J, Katz B. (1954) Quantal components of the end-plate potential. J Physiol 124:560-573.

Del Castillo J, Katz B. (1954) Changes in end-plate activity produced by pre-synaptic polarization. J Physiol 124:560-573.

Del Castillo J, Stark . (1952) The effect of calcium ions on the motor end-plate potentials. J Physiol 116:507-515.

DeMaria CD, Soong TW, Alseikhan BA, Alvania RS, Yue DT. (2001) Calmodulin bifurcates the local Ca^{2+} signal that modulates P/Q-type Ca^{2+} channels. Nature 411:484-489.

Diaz-Rojas F, Sakaba T, Kawaguchi S. (2015) Ca^{2+} current facilitation determines short-term facilitation at inhibitory synapses between cerebellar Purkinje cells. J Physiol 593 4889–494.

Eccles JC. (1961) The mechanism of synaptic transmission. Ergebn Physiol 51:299-430.

Eccles JC. (1964) The physiology of synapses. Springer-Verlag, 1964.

Edwards FA, Konnerth A, Sakmann B, Takahashi T. (1989) A thin slice preparation for patch clamp recordings from neurones of the mammalian central nervous system. Pflugers Arch 414:600-612.

Edwards FA, Konnerth A, Sakmann B. (1990) Quantal analysis of inhibitory synaptic transmissionin the dentate gyrus of rat hippocampal slices: a patch-clamp study. J Physiol 430:213-249.

Fatt P, Katz B. (1951) An analysis of the end-plate potential recorded with an intra-cellular electrode. J Physiol 115:320-370.

Feng TP. (1988) Looking back, looking forward. Ann Rev Neurosci 11:1-13.

Hagiwara S, Tasaki I. (1958) A study on the mechanism of impulse transmission across the giant synapse of the squid. J Physiol 143:114-137.

Hamill OP, Marty A, Neher E, Sakmann B, Sigworth FJ. (1981) Improved patch-clamp techniques for high resolution current recording from cells and cell-free membrane patches. Pflugers Arch 391:85-100.

Herman MA, Ackermann F, Trimbuch T, Rosenmund C. (2014) Vesicular glutamate transporter expression level affects synaptic vesicle release probability at hippocampal synapses in culture. J Neurosci 34:11781-11791.

Hodgkin A, Huxley AF. (1952) A quantitative description of membrane current and its application to conduction and excitation in nerve. J Physiol 117:500-544.

Hori T, Takahashi T. (2009) Mechanisms underlying short-term modulation of transmitter release by presynaptic depolarization. J Physiol 587:2987-3000.

Hori T, Takahashi T. (2012) Kinetics of synaptic vesicle refilling with neurotransmitter glutamate. Neuron 76:511-517.

Ishikawa T, Sahara Y, Takahashi T. (2002) A single packet of transmitter does not saturate postsynaptic glutamate receptors. Neuron 34:613-621.

Ishikawa T, Kaneko M, Shin H-S, Takahashi T. (2005) Presynaptic N-type and P/Q-type Ca^{2+} channels mediating synaptic transmission at the calyx of held of mice. J Physiol 568:199-209.

Iwasaki S, Takahashi T. (1998) Developmental changes in calcium channel types mediating synaptic transmission in rat auditory brainstem. J Physiol 509:419-423.

Jack JJ, Redman SJ, Wong K. (1981) The components of synaptic potentials evoked in cat spinal motoneurones by impulses in single group Ia afferents. J Physiol 321:65-96.

Jonas P, Major G, Sakmann B. (1993) Quantal components of unitary EPSCs at the mossy fibre synapse on CA3 pyramidal cells of rat hippocampus. J Physiol 472:615-663.

Katz B. (1993) On neurotransmitter secretion. Interdiscip Sci Rev 18:359-364.

Katz B, Miledi R. (1963) A study of spontaneous miniature potentials in spinal motoneurones. J Physiol 168:389-422.

Katz B, Miledi R. (1967) A study of synaptic transmission in the absence of nerve impulses. J Physiol 192:407-436.

Katz B, Miledi R. (1968) The role of calcium in neuromuscular facilitation. J Physiol 195:481-492.

Katz B, Miledi R. (1969) Tetrodotoxin-resistant electric activity in presynaptic terminals. J Physiol 203:459-487.

Klein M, Kandel ER. (1978) Presynaptic modulation of voltage-dependent Ca^{2+} current: mechanism for behavioral sensitization in *Aplysia californica*. Proc Natl Acad Sci U S A 75:3512-3516.

Koike-Tani M, Kanda T, Saitoh N, Yamashita T, Takahashi T. (2008) Involvement of AMPA receptor desensitization in short-term synaptic depression at the calyx of held in developing rats. J Physiol 586:2263-2275.

Kojima H, Takahashi T. (1985) Characterization of miniature inhibitory post-synaptic potentials in rat spinal motoneurones. J Physiol 368:627-640.

Kriebel ME. (1978) Small mode miniature end plate potentials are increased and in fatigued preparations and in high Mg^{2+} saline. Brain Res 148:381-388.

Kuno M. (1995) The synapse: function, plasticity, and neurotrophism. Oxford Univ Press, 1995.

Larkman A, Hannay T, Stratford K, Jack J. (1992) Presynaptic release probability influences the locus of long-term potentiation. Nature 360:70-73.

Liu G, Choi S, Tsien RW. (1999) Variability of neurotransmitter concentration and nonsaturation of postsynaptic AMPA receptors at synapses in hippocampal cultures and slices. Neuron 22:395-409.

Llinas R, Steinberg IJ, Walton K. (1976) Presynaptic calcium currents and their relation to synaptic transmission: voltage clamp study in squid giant synapse and theoretical model for the calcium gate. Proc Natl Acad Sci U S A 73:2918-2922.

Llinas R, Sugimori M, Silver RB. (1992) Microdomains of high calcium concentration in a presynaptic terminal. Nature 256:677-679.

Miledi R. (1973) Transmitter release induced by injection of calcium ions into nerve terminals. Proc R Soc B 183:421-425.

Miledi R, Slater CR. (1966) The action of calcium on neuronal synapses in the squid. J Physiol 184:473-498.

Muller M, Felmy F, Schneggenburger R. (2008) A limited contribution of Ca^{2+} current facilitation to paired-pulse facilitation of transmitter release at the rat calyx of held. J Physiol 585:5503-5520.

Nakamura Y, Harada H, Kamasawa N, Matsui K, Rothman JS, Shigemoto R, Silver AR, DiGregorio DA, Takahashi T. (2015) Nanoscale distribution of presynaptic Ca^{2+} channels and its impact on vesicular release during development. Neuron 85:145-158.

Nicholls J, Wallace BG. (1978) Quantal analysis of transmitter release at an inhibitory synapse in the central nervous system of the leech. J Physiol 281:171-185.

Sahara Y, Takahashi T. (2001) Quantal components of the excitatory postsynaptic currents at a rat central auditory synapse. J Physiol 536:189-197.

Silver RA, Cull-Candy SG, Takahashi T. (1996) Non-NMDA glutamate receptor occupancy and open probability at a rat cerebellar synapse with single and multiple release sites. J Physiol 494:231-250.

Takahashi T. (1978) Intracellular recording from visually identified motoneurons in rat spinal cord slices. Proc R Soc B 202:417-421.

Takahashi T. (1984) Inhibitory miniature synaptic potentials in rat motoneurons. Proc R Soc B 221:103-110.

Takahashi T. (1992) The minimal inhibitory synaptic currents evoked in neonatal rat motoneurones. J Physiol 450:593-611.

Takahashi T, Forsythe I, Tsujimoto T, Barnes-Davies M, Onodera K. (1996) Presynaptic calcium current modulation by a metabotropic glutamate receptor. Science 274:594-597.

Takami C, Eguchi K, Hori T, Takahashi T. (2017) Impact of vesicular glutamate leakage on synaptic transmission at the calyx of held. J Physiol 595:1263-1271.

Takeuchi A, Takeuchi N. (1962) Electrical changes in pre- and postsynaptic axons of the giant synapse of *Loligo*. J Gen Physiol 45:1181-1193.

Tauc L. (1982) Nonvesicular release of neurotransmitter. Physiol Rev 62:857-893.

Tsujimoto T., Jeromin A., Saitoh N., Roder J.C., Takahashi T.. (2002) Neuronal calcium sensor 1 and activity-dependent facilitation of P/Q type calcium currents at presynaptic nerve terminals. Science 295:2276-2279.

Wang L, Tu P, Bonet L, Aubrey KR, Supplisson S. (2013) Cytosolic transmitter concentration regulates vesicle cycling at hippocampal GABAergic terminals. Neuron 80:143-158.

Yamashita M, Kawaguchi S, Hori T, Takahashi T. (2018) Vesicular GABA uptake can be rate limiting for recovery of IPSCs from synaptic depression. Cell Rep 22:3134-3141.